

Cover Page



Universiteit Leiden



The handle <http://hdl.handle.net/1887/138650> holds various files of this Leiden University dissertation.

Author: Junaid, A.O.

Title: Microengineered human blood vessels for next generation drug discovery

Issue date: 2020-12-16

Chapter IV

Ebola hemorrhagic shock syndrome-on-a-chip

Abidemi Junaid, Huaqi Tang, Anne van Reeuwijk, Yasmine Abouleila, Petra
Wuelfroth, Vincent van Duinen, Wendy Stam, Anton Jan van Zonneveld, Thomas
Hankemeier, Alireza Mashaghi

iScience (2020) **23**, 100765

Chapter IV

Abstract

Ebola virus, for which we lack effective countermeasures, causes hemorrhagic fever in humans, with significant case fatality rates. Lack of experimental human models for Ebola hemorrhagic fever is a major obstacle that hinders the development of treatment strategies. Here, we model the Ebola hemorrhagic syndrome in a microvessel-on-a-chip system and demonstrate its applicability to drug studies. Luminal infusion of Ebola virus-like particles leads to albumin leakage from the engineered vessels. The process is mediated by the Rho/ROCK pathway and is associated with cytoskeleton remodelling. Infusion of Ebola glycoprotein (GP_{1,2}) generates a similar phenotype, indicating the key role of GP_{1,2} in this process. Finally, we measured the potency of a recently developed experimental drug FX06 and a novel drug candidate, melatonin, in phenotypic rescue. Our study confirms the effects of FX06 and identifies melatonin as an effective, safe, inexpensive therapeutic option that worth investigating in animal models and human trials.

Introduction

Ebola hemorrhagic fever is a rapidly progressive and highly fatal condition for which there is no established treatment [1]. The Ebola epidemic in West Africa (2014-2016) was a health crisis of unprecedented magnitude and impact, causing more than 11,000 deaths and destabilizing three countries [2]. Currently, World Health Organization and African countries are struggling to contain a new large outbreak in Africa, which has led to hundreds of deaths [3]. Vascular integrity impairment with subsequent blood volume loss (the so-called shock syndrome) is the primary cause of death in Ebola patients. Despite supportive care, more than 50% of patients die, with significant interindividual differences in disease outcome reported and attributed to viral loads and host factors [4, 5]. Despite progress, many challenges remain to be addressed, including improving early diagnosis, predicting disease progression, and developing therapeutic and preventive methods.

The lack of experimental models and sensitive detection tools has historically hindered the early detection of Ebola vasculopathy and the development of Ebola drugs. However, rodent models that can mimic certain aspects of Ebola disease in humans have been developed and are now used along with monkey models as *in vivo* models of the disease [6-8]. The use of these models has recently led to the development of experimental therapeutic strategies, including small molecules [9], antibodies [10-13] and nanoparticles [14], as well as glycofullerenes [15]. However, these therapeutics do not directly target hemorrhagic shock syndrome but rather Ebola virus infection. Additionally, animal models are costly and cannot fully recapitulate the physiology and pathology of human organs, making it difficult to predict the efficacy, safety and toxicity of experimental Ebola drugs [16].

In vitro human models for viral hemorrhagic shock syndrome are currently lacking. However, such models would not only be useful for studying the pathogenesis of Ebola in a human-like setting but would also be critical for diagnostics and drug development. Chip-based disease models are becoming important research tools in biology and medicine [17-19]. Examples include the modeling of drug toxicity-induced pulmonary edema in a lung-on-a-chip model [20], the modeling of Alzheimer's disease in a brain-on-a-chip platform [21] and the simulation of diabetic nephropathy in a glomerulus-on-a-chip microdevice [22]. Additionally, there is a growing interest in using *in vitro* engineered models in vascular medicine [23-39], yet no chip-based model of viral hemorrhagic shock syndrome has been introduced. Here, we develop,

for the first time, a microvessel-on-a-chip based model of Ebola (species Zaire ebolavirus) viral hemorrhagic syndrome and demonstrate its usefulness by exploring the signaling and physical processes that underlie the hemorrhagic syndrome and by targeting those processes using drug candidates.

Transparent Methods

Chip design

We designed a novel chip structure (T-design) based on the MIMETAS OrganoPlate platform. This new design involves a T-junction shown in Figure 1 in which the channels are separated by a phaseguide (Vulto et al., 2011). The design, due to its geometry, enables easy generation of leak tight vessels and quantification of vascular leakage. With the T-design there is a small area that has direct contact with the ECM, which makes it easy to create leak tight vessels compared to if a larger area of the microvessel has contact with the ECM. Additionally, this likely increases the duration of the permeability measurement before the system becomes saturated. Fabrication of the glass chipsets was carried out by MIMETAS using a previously established protocol (Vulto et al., 2011).

Cell culture

Human umbilical vein endothelial cells (HUVECs) were cultured in Endothelial Cell Growth Medium 2 (C-39216; PromoCell). We used the T-design OrganoPlate for all microfluidic cell culture. Thus, the microvascular and extracellular matrix (ECM) channels were separated by phaseguides. Before seeding the cells, 4 mg/ml rat tail collagen type 1 (3440-005-01; Trevigen) neutralized with 10% 37 g/L Na₂CO₃ (S5761; Sigma) and 10% 1 M HEPES buffer (15630-056; Gibco) was added in the ECM channels. Subsequently, the collagen was let to polymerize by incubating the device for 10 minutes in the incubator at 37°C and 5% CO₂. The observation windows were filled with 50 µl Hank's Balanced Salt Solution with calcium and magnesium buffers (HBSS+; 24020117; Life Technologies) for optical clarity and to prevent gel dehydration. We trypsinized cells at 80-90% confluency and seeded 20·10⁶ cells/ml in gelatin-coated microvascular channels of the OrganoPlate. Afterwards, the cells were incubated at

37°C and 5% CO₂ for one hour to allow microvascular formation. After incubation, 50 µl of culture medium was added to the inlets and outlets of the microvascular channels. The device was placed on a rocker platform with a 7° angle of motion and an eight-minute timed operation to allow continuous flow of medium in the microvessels. After 24 h, the medium was refreshed, and the HUVECs were cultured for an additional 3-4 days.

Permeability assay

Endothelial cell culture medium was spiked with U46619 (D8174; Sigma), Ebola virus-like particles (VLPs; ZEBO-VLP; The Native Antigen Company) and the Ebola virus envelope glycoprotein (GP_{1,2}; EBOVKW95-ENV; The Native Antigen Company). The Ebola VLPs were diluted in 0.2% Endothelial Cell Growth Medium 2 to the desired experimental concentrations. RevitaCell™ Supplement (A2644501; ThermoFisher), FX06 (F4 Pharma GmbH) and melatonin (M5250; Sigma) were used to treat vessel permeability. To prevent the degradation of FX06 in the microvessels, 100 nM carboxypeptidase inhibitor (C0279; Sigma) was added.

To measure vessel permeability, the ECM channel inlets were refreshed with 20 µl HBSS+. Then, the media in the inlets and outlets of the microvascular channels were replaced with 40 µl and 30 µl, respectively, of 125 µg/ml Alexa Fluor 555-conjugated albumin (A34786; Life Technologies). Next, the OrganoPlate was placed in the environmental chamber (37°C; 5% CO₂) of a fluorescence microscope system (Nikon Eclipse Ti), and time-lapse images were captured.

We calculated the permeability coefficient by determining the fluorescence intensities in the microvascular (I_p) and ECM (I_g) channels of the captured images and normalizing them to each other at each time point. This calculation showed the change in the intensity ratio inside the gel channel as a function of time. The area of the ECM channel (A_g) was $480 \cdot 10^{-6} \text{ cm}^2$, and the length of the vessel wall between the ECM and microvascular regions (l_w) was $400 \cdot 10^{-4} \text{ cm}$. The scatter plot was fitted with a linear trend line to determine the slope, and the apparent permeability was calculated as follows:

$$P_{app} (\cdot 10^{-6} \text{ cm/s}) = \frac{d\left(\frac{I_g}{I_p}\right)}{dt} \cdot \frac{A_g}{l_w}$$

Immunohistochemistry

The medium was aspirated from the medium inlets, and the chip outlets and cells were fixed using 4% paraformaldehyde (PFA) in HBSS+ for 10 minutes at room temperature. The fixative was aspirated, and the cells were rinsed once with HBSS+. Next, the cells were permeabilized for two minutes with 0.2% Triton X-100 in HBSS+ and washed once with HBSS+. The cells were blocked in 5% BSA in HBSS+ for 30 minutes and incubated with the primary antibody solution overnight at 4°C. Mouse anti-human CD144 (1:100; 555661; BD Biosciences) and mouse anti-human CD62E (25µg/ml; BBA26-200; R&D Systems) were used as the primary antibodies. The wells were washed with HBSS+, followed by a one-hour incubation with Hoechst (1:2000; H3569; Invitrogen), rhodamine phalloidin (1:200; P1951; SIGMA) and the secondary antibody solution, containing an Alexa Fluor 488-conjugated goat-anti-mouse antibody (1:250; R37120; Waltham). The wells were washed three times with HBSS+. High-quality Z-stack images of the stained cells were acquired using a high-content confocal microscope (Molecular Devices, ImageXpress Micro Confocal). Quantification of Pearson's correlation coefficient for the co-localization of VE-cadherin and F-actin was performed using Coloc2 (ImageJ). Results are depicted as means ± SEMs (n=2).

Statistical analysis

We used IBM SPSS Statistics 23 for statistical analyses. Outliers in the box plots were identified by SPSS. The plotted data are the means ± SEMs of three or four biological replicates. Multiple comparisons were performed by one-way ANOVA followed by Dunnett's t-test. The results were considered significant at *P < 0.05, **P < 0.01 and ***P < 0.001.

Results

Here, we describe a simple chip-based model of Ebola-induced vascular integrity loss. To provide the proof-of-principle for this approach and to ensure that the platform can be extended to a low-cost, easy-to-use high-throughput platform for diagnostics, we included the minimal components needed to model the process. We first generated microvessels within the fabricated OrganoPlates (T-design) using human endothelial cells (primary HUVECs) at the interface of a collagen type 1 network. The chip design allowed us to culture 96 microvessels with heights of 120 μm and widths of 400 μm (see Figure 1a-d). To develop the model and generate all the data for the current study, we have used approximately a total of 550 independent chips. To ensure that the engineered vessel recapitulated the physiological barrier function of a natural vessel, we measured the transport of albumin across the endothelial wall into the collagen network. In a physiological setting, the vessel is expected to be impermeable but to respond dynamically to physiological stimuli. Permeability experiments were carried out after incubating the microvessels with and without histamine (an endogenous biogenic amine known to induce vascular permeability during inflammatory processes) for 40 or 60 minutes. As shown in Figure 1e, we observed no leakage of albumin from the engineered vessels (control; without stimuli) within a 10-minute interval during the permeability assay. Permeability was, however, induced by the administration of histamine, indicating that the endothelial wall is not passive and responds to stimuli as expected (see Figure 1e-g).

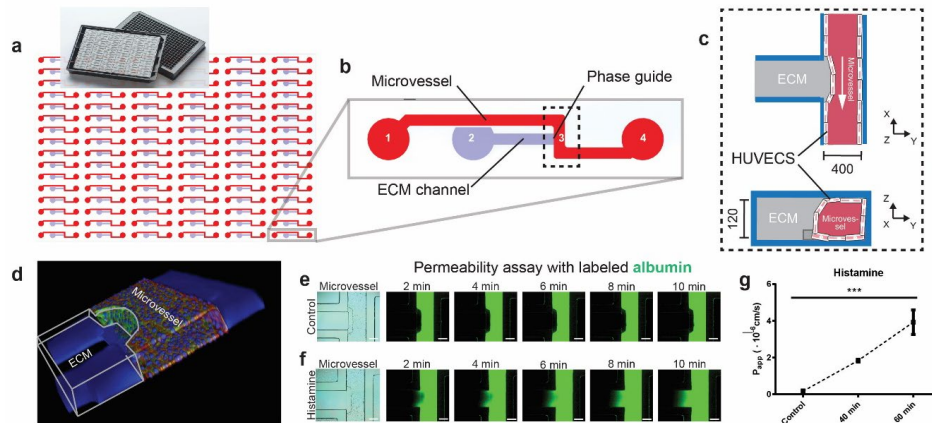


Figure 1 | Viral hemorrhagic syndrome-on-a-chip. (a) Schematic diagram of the 96 microfluidic devices composing the gradient design (T-design) in the OrganoPlate, based on a 384 wells plate interface on top and 96 microfluidic devices integrated in the bottom. (b) Each microfluidic tissue chip consists of a microvessel compartment with medium inlet (1) and outlet (4), gel inlet (2) and observation window (3). The dashed highlighted rectangular box indicates the region depicted in c. (c) Diagram of the monolayers of human umbilical vein endothelial cells (HUVECs) forming a microvessel next to the ECM in the microfluidic system. (d) A 3D reconstruction showing the human microvessel-on-a-chip that was formed by cultured HUVECs (red, F-actin) and demonstrated continuous on-chip junctions (green, VE-cadherin). (e) Time-lapse fluorescence images of albumin (green) perfusion in the microvessel channel. Scale bar, 200 μm . (f) 100 μM histamine was pipetted in the medium inlet and outlet of the microfluidic device and incubated for 60 minutes under perfusion with the Mimetas rocker platform. Subsequently, labeled albumin (green) was added to the medium inlet and outlet and time-lapse fluorescence images of albumin (green) diffusing from the microvessel to the ECM channel were taken. Scale bar, 200 μm . (g) Apparent permeability (P_{app}) of microvessels in the time response to 100 μM histamine. The control is microvessel without histamine treatment. Data are represented as mean \pm SEM.

Next, we infused various concentrations of VLPs to determine whether VLPs alone are sufficient to induce permeability and whether the extent of permeability is viral load-dependent. Infusion of VLPs led to a dramatic increase in the permeability of the engineered microvessels, as shown in Figure 2a and b. The VLPs used in these experiments were non-replicating, indicating that the viral components interact directly with endothelial cells and affect their barrier function, presumably by affecting cellular mechanics and intercellular interactions. Immunostaining of F-actin indicated that Ebola VLPs indeed alter the mechanics and physical interaction of endothelial cells, explaining the induction of permeability (see

Figure 2c). However, treatment with VLPs did not result in an apparent rearrangement of VE-cadherin but instead caused a clear increase in actin stress fiber formation, consistent with the findings in previous reports [40]. Moreover, we observed significant upregulation of E-selectin, a mediator of immune cell recruitment and a biomarker for endothelial dysfunction, clearly indicating the activation of the engineered endothelium (see Supplementary figure 1).

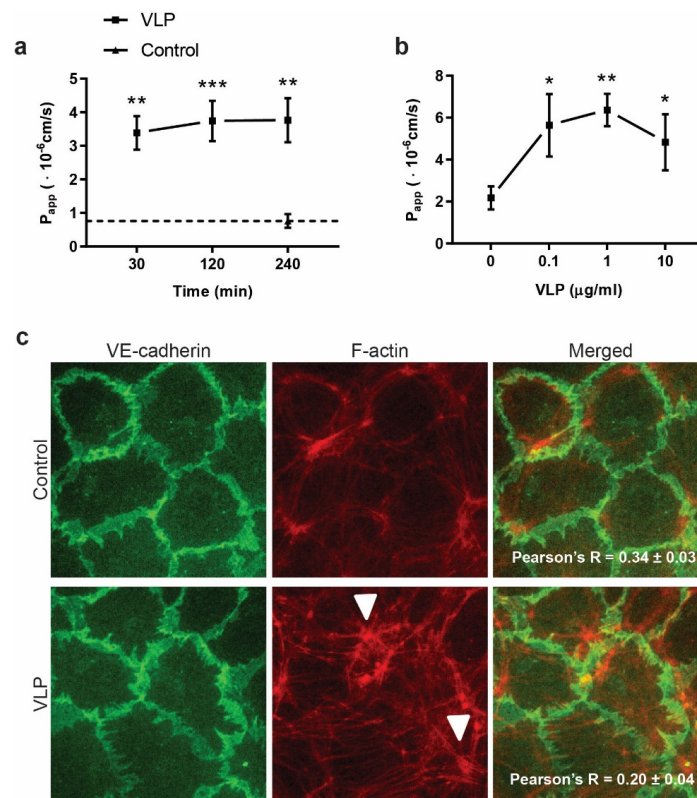


Figure 2 | Microvascular dysfunction in the viral hemorrhagic shock syndrome-on-a-chip platform. (a) Apparent permeability (P_{app}) of microvessels in response to Ebola VLPs at several time points. Microvessels were exposed to 1 $\mu\text{g/ml}$ VLPs, followed by a permeability assay. (b) Concentration dependence of the VLP effect. Microvessels were treated for 2 h with the indicated concentrations of VLPs, followed by a permeability assay. (c) Endothelial cells stained for VE-cadherin (green) and F-actin (red) after exposure to 1 $\mu\text{g/ml}$ VLPs for 2 h. A moderate increase in actin filament stress fiber formation was observed (arrowheads). Pearson's correlation coefficient was lower in microvessels exposed to Ebola VLPs than in the control, showing an increase in stress fiber formation and endothelial cell activation. Data are represented as mean \pm SEM.

Chapter IV

Next, we assessed whether VLPs affect cellular mechanics by modulating the Rho/ROCK pathway. Over-activation of the Rho/ROCK pathway is an underlying mechanism of several vasculopathies, including endotoxin-induced septic vasculopathy [41-43]. Given that some of the major pathophysiological mechanisms of Ebola virus disease resemble those of bacterial septic shock [44, 45], it is conceivable that the Rho/ROCK pathway may also play a critical role in the pathogenesis of the severe vascular leak observed in Ebola disease [46]. To test this hypothesis, we first determined whether we could stimulate the Rho/ROCK pathway in our engineered system and generate a phenotype similar to that observed after the infusion of Ebola VLPs. We used U46619, a small molecule that activates the Rho/ROCK pathway, and measured the time- and concentration-dependent response of the vessels [47]. Treatment of the microvessels with U46619 (10 μ M) increased permeability significantly (see Figure 3a). As the concentration of U46619 increased, the barrier permeability progressively increased (see Figure 3b). Immunostaining of F-actin revealed induced alterations in the cellular cytoskeleton associated with the disruption of the endothelial barrier (see Figure 3c).

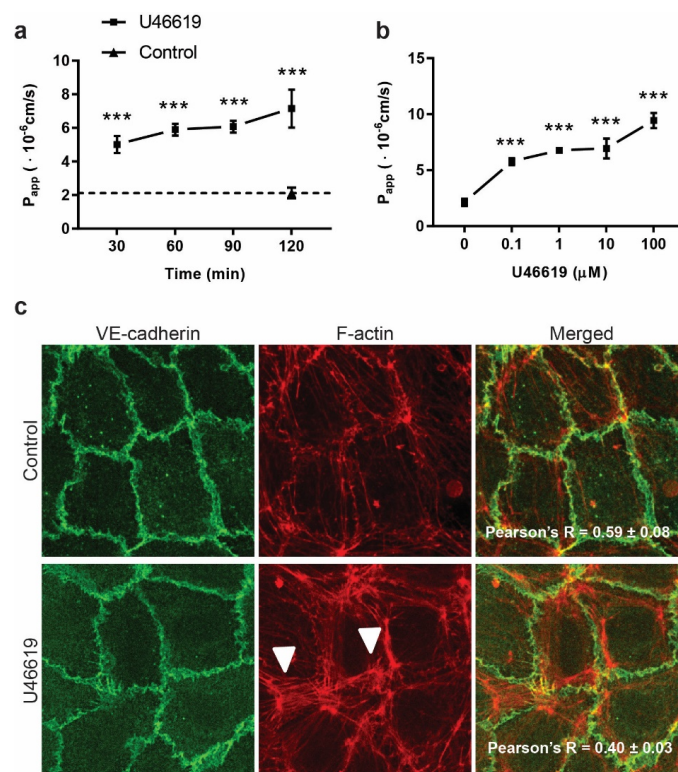


Figure 3 | U46619 induces vascular permeability in the microvessel-on-a-chip platform. (a) Time dependence of U46619-induced barrier opening. Microvessels were exposed to 10 μ M U46619, followed by a permeability assay. **(b)** Dose response to U46619 in microvessels. Microvessels were treated with several concentrations of U46619 for 1 h to measure permeability. **(c)** Immunofluorescence micrographs of on-chip cultured endothelium. After treatment for 1 h with 10 μ M U46619, endothelial cells were stained for VE-cadherin (green) and F-actin (red). An increase in actin stress fiber formation was observed (arrowheads). Pearson's correlation coefficient was lower in microvessels exposed to U46619 than in the control, showing an increase in stress fiber formation and endothelial cell activation. Data are represented as mean \pm SEM.

Subsequently, we investigated whether Rho/ROCK pathway inhibition suppresses the Ebola VLP-induced vascular phenotype. As RevitaCell™ Supplement [48] is known to specifically inhibit ROCK, we investigated whether this compound could reverse the Ebola VLP-induced phenotype. We compared vascular permeability of the microvessels-on-chips exposed to Ebola VLPs only with permeability of microvessels exposed to Ebola VLPs and RevitaCell™ Supplement simultaneously to inhibit the Rho/ROCK pathway. We observed a full suppression

of the VLP-induced permeability upon administration of the inhibitor together with the VLPs (see Figure 4). This result shows that Ebola VLPs critically modulate the Rho/ROCK pathway in hemorrhagic shock syndrome.

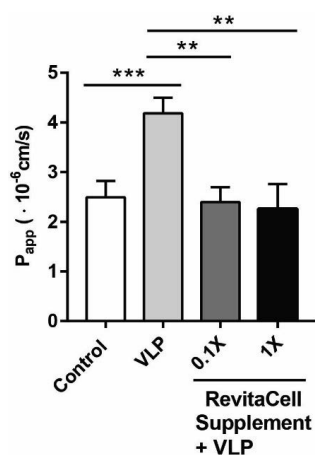


Figure 4 | ROCK-specific inhibitor treatment abolishes VLP-induced vascular permeability. Microvessels were either left untreated, incubated with 1 μ g/ml Ebola VLPs or exposed to both RevitaCell™ Supplement (0.1 and 1 \times) and 1 μ g/ml Ebola VLPs simultaneously, with an incubation time of 2 h. Data are represented as mean \pm SEM.

Existing evidence suggests that Ebola virus envelope glycoprotein GP_{1,2} is a key mediator of viral pathogenesis and a determinant of disease severity [49]. To test whether GP_{1,2} alone could simulate Ebola VLPs effect, we infused purified GP_{1,2} into our engineered vessels and measured the dose and time responses. Figure 5a shows that stimulation with 100 ng/ml GPs_{1,2} for 120 and 240 minutes led to a significant increase in vessel permeability. Moreover, we measured the dose-response curve using the chip platform (see Figure 5b). Importantly, the increased permeability of GPs_{1,2}-treated microvessels was associated with the formation of stress fibers (see Figure 5c). These results directly show the ability of Ebola GP_{1,2} to induce vasculopathy and indicate that our chip-based model can detect both VLP-induced and GPs_{1,2}-induced vascular permeability.

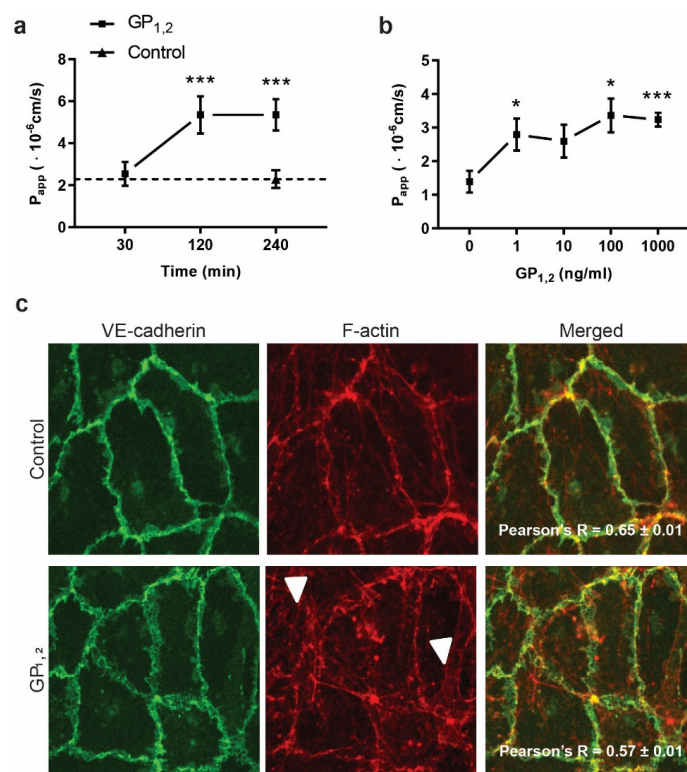


Figure 5 | Endothelial cell activation induced by the Ebola glycoprotein. (a) Permeability assay of microvessels exposed to 100 ng/ml GP_{1,2} at the indicated time points. **(b)** Dose response to GP_{1,2}. Microvessels were incubated with GP_{1,2} at the indicated concentrations for 2 h to measure permeability. **(c)** Immunostaining of endothelial cells for VE-cadherin (green) and F-actin (red) after treatment with 100 ng/ml GP_{1,2}. A moderate increase in actin stress fiber formation was observed (arrowheads). Pearson's correlation coefficient was lower in microvessels exposed to Ebola GPs_{1,2} than in the control, showing an increase in stress fiber formation and endothelial cell activation. Data are represented as mean ± SEM.

To demonstrate the applicability of our chip-based assay to pharmacological studies, we used this platform to study the effect of two potential drugs. According to our simple working model, Ebola virus stimulates the Rho/ROCK pathway, thereby inducing actin bundle formation and a tensile force that loosens the intercellular junctions formed by VE-cadherin. We targeted this process at two levels: (1) Rho/ROCK signaling (intracellular), via melatonin; and (2) VE-cadherin (extracellular) and the associated actin bundles, via FX06 (see Figure 6a) [50-52]. We found that both molecules effectively suppress vasculopathy and further showed

that FX06, which binds to VE-cadherin, thus reducing adhesion, also affects actin bundle formation directly (or indirectly via Fyn-mediated signaling[53]) (Supplementary figure 2). Treatment with FX06 counteracted vascular leakage in VLP-treated vessels, which is consistent with the results of previous animal experiments [54] and the clinical benefit noted in a case report [55] (see Figure 6b). However, vascular integrity was not directly measured in any previous study. Similarly, melatonin reduced vascular permeability in our viral hemorrhagic shock syndrome-on-a-chip model (see Figure 6c and Supplementary figure 3).

IV

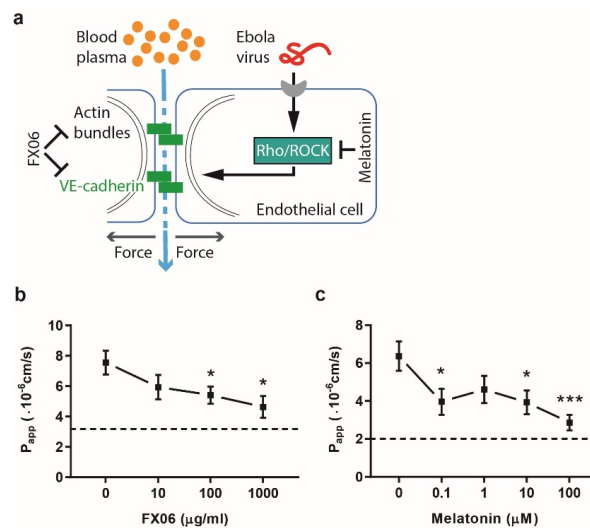


Figure 6 | FX06 and melatonin effectively ameliorate vascular integrity loss in the Ebola hemorrhagic shock syndrome-on-a-chip model. (a) FX06 and melatonin rebalance mechanical forces in endothelial cells to restore vascular integrity in Ebola viral hemorrhagic shock syndrome. **(b)** Microvessels exposed to 1 μg/ml Ebola VLPs were treated with FX06 at the indicated concentrations for 2 h. Subsequently, a permeability assay was carried out. **(c)** Dose response to melatonin in microvessels exposed to 1 μg/ml Ebola VLPs for 2 h, followed by a permeability assay. Data are represented as mean ± SEM.

A similar effect of melatonin was also observed when we stimulated the Rho/ROCK pathway with U46619 (Supplementary figure 4). This observed effect of melatonin is intriguing, as the effect of melatonin on the permeability of vessels has been previously reported in the context of cancer and septic shock, and the function of melatonin has been attributed to Rho/ROCK pathway modulation and subsequent changes to the cytoskeletal elements including actin

Chapter IV

stress fibers [56, 57]. Melatonin has been proposed as a potential drug for Ebola hemorrhagic shock [58-60] but has never been tested experimentally. Given that melatonin is a natural molecule in the body and is safe when administered for at least a year [61] and given our observation that melatonin effectively suppresses the Ebola-induced loss of vascular integrity, our study suggests that melatonin is a promising drug for treating Ebola hemorrhagic shock syndrome. However, additional investigations are required to confirm the clinical therapeutic efficacy of melatonin.

Discussion

Vasculopathy is a critical and fatal consequence of Ebola virus infection [62-64]. Despite extended *in vivo* studies, the underlying molecular mechanisms are still elusive, no effective cure is available, and treatment strategies are primarily palliative. To discover and develop new drugs for Ebola in a cost-effective manner with high predictive power, microengineered disease models of human organs are needed. The hemorrhagic shock syndrome-on-a-chip described here is the first of its kind. Despite its simplicity, this model is robust, with significant fidelity in mimicking, at least partly, the structure and functions of human microvessels and Ebola disease-associated vasculopathy. This platform permitted high-throughput simulation of the vascular permeability induced by Ebola VLPs and Ebola GP_{1,2} as well as an increased surface expression of E-selectin which mediates disseminated intravascular coagulation, and death [58, 65].

Our study provides direct evidence for the usefulness of two candidate drugs, FX06 (which directly targets mechanical elements [66]) and melatonin (which directly targets biochemical signaling [67]), for treating Ebola patients. Although melatonin and FX06 are not antiviral molecules, they can be used to reduce the severity of hemorrhagic shock syndrome. Melatonin has not been used clinically to treat Ebola before, however, it was used routinely in other several clinical settings in humans [68]. Intravenous administration of 60 mg melatonin (equivalent to ~100 μ M in blood) is believed to be safe and with no complications [69, 70]. This indicates that the highest concentration of melatonin (100 μ M) used in our study is considered safe and can be translated to future clinical applications. Similarly, the highest

concentration of FX06 in our model is clinically relevant and has been used clinically to treat one Ebola patient [55].

Our *in vitro* model will help in understanding the underlying mechanisms of melatonin and FX06. This will allow the development of new compounds capable of delaying the effect of Ebola-induced vascular leakage. Additionally, the model can be of help in screening for therapeutic monoclonal antibodies[71, 72], in which the effect of antibodies targeting endothelial cells or VLPs to block the interaction between the two can be assayed. Finally, we stress the importance of the dose-response analysis enabled by the proposed platform. Recently, some Ebola drugs such as favipiravir have been abandoned because of problems with dosing [73]. The developed *in vitro* model can aid in the efforts to develop an effective pharmacokinetic model of drug treatments, and therefore, assist in designing the proper dose regimens. This chip-based platform will thus be a valuable tool complementing state-of-the-art technologies for combating current and future Ebola outbreaks.

Limitations of the Study

We note that this study has certain limitations that will be addressed in our future studies. The bidirectionality of the flow in the microvessels is one of the limitations in our system. Currently, we are developing a perfusion pump, which can provide a unidirectional flow for each microvessel channel by covering the whole plate, to solve this problem. We, however, anticipate that the observed vascular permeability remains largely unaffected by the flow directionality, as our preliminary analysis shows (Supplementary figure 5). The proposed approach is high-throughput, yet the analysis time can be further reduced using high content imaging systems.

Our approach allows us to disentangle the direct contribution of VLPs and viral proteins to vascular integrity loss from the contributions of host immunity (indirect mechanism) and the process of infection. The proposed *in vitro* model can be used in future to address the contributions of immune cells and to study endothelial cell infection. Shed glycoproteins from infected macrophages and dendritic cells can be readily assayed using the proposed approach. The engineered vessels can be further improved by including tissue specific ECM and other vascular cells (e.g., pericytes). The pharmacological analysis can be further extended to

Chapter IV

investigate the kinetics of recovery (after titration of the inhibitors) in the proposed in vitro model and to translate the results to nonhuman primate and human settings. Certain control and complementary experiments need to be performed (e.g., testing VP40-only VLPs) before exploring the translatability of the results. The platform can also be adapted to investigate therapeutic antibodies and other drug options. Finally, this study will contribute to understanding and detection of other highly dangerous viral infections that cause hemorrhagic shock including Lassa and Dengue.

Acknowledgments

We are grateful to Cesar Munoz-Fontela, Tom Ottenhoff, Marielle Haks, Beatriz Escudero-Perez, and Viktor Volchkov for discussions. We thank F4 Pharma GmbH for the generous gift of FX06. AM and YA acknowledge the support by the Leiden University Fund (W19340-5-EML) and Netherlands Organization for Scientific Research (NWA.1228.191.329). HT is financially supported by the CSC Scholarship offered by the China Scholarship Council. AJ, TH and AJvZ were financially supported by the RECONNECT CVON Groot consortium, which is funded by the Dutch Heart Foundation and TH, AJvZ and VvD were supported by a ZonMW MKMD grant (114022501). AM, TH and HT acknowledge the support by the Netherlands Organization for Scientific Research (NWO-TTW, grant number 16249).

Author contributions

AM conceived, designed and supervised the research. AJ, HT, AvR, and YA performed the experiments. WS helped with the immunostaining. AJ, HT and AM analysed the data. AM, HT, and AJ wrote the paper. All authors participated in the revisions of the manuscript and read and approved the final version.

Declaration of interests

Authors declare no conflict of interest related to the content of this manuscript. T.H. is shareholder in Mimetas BV, which was involved in the fabrication of the chips used in this study.

References

1. Jameson, J.L., et al., *Harrison's Principles of Internal Medicine (20th Edition)*. 2018: McGraw-Hill Education.
2. Nicholas G. Evans, T.C.S., Maimuna S. Majumder, *Ebola's Message: Public Health and Medicine in the Twenty-First Century*. 2016: The MIT Press.
3. Dyer, O., *Congo's Ebola epidemic is now its worst ever and still spreading*. BMJ, 2019. **364**.
4. de La Vega, M.A., et al., *Ebola viral load at diagnosis associates with patient outcome and outbreak evolution*. Journal of Clinical Investigation, 2015. **125**(12): p. 4421-4428.
5. Hartley, M.A., et al., *Predicting Ebola Severity: A Clinical Prioritization Score for Ebola Virus Disease*. Plos Neglected Tropical Diseases, 2017. **11**(2).
6. Willyard, C., *Advances in marmoset and mouse models buoy Ebola research*. Nature Medicine, 2014. **20**(12): p. 1356-1357.
7. Bennett, R.S., et al., *Nonhuman Primate Models of Ebola Virus Disease*. Marburg- and Ebolaviruses: From Ecosystems to Molecules, 2017. **411**: p. 171-193.
8. de la Vega, M.A., et al., *Modeling Ebola Virus Transmission Using Ferrets*. Msphere, 2018. **3**(5).
9. Warren, T.K., et al., *Therapeutic efficacy of the small molecule GS-5734 against Ebola virus in rhesus monkeys*. Nature, 2016. **531**(7594): p. 381-+.
10. Qiu, X.G., et al., *Characterization of Zaire ebolavirus glycoprotein-specific monoclonal antibodies*. Clinical Immunology, 2011. **141**(2): p. 218-227.
11. Qiu, X.G., et al., *Successful Treatment of Ebola Virus-Infected Cynomolgus Macaques with Monoclonal Antibodies*. Science Translational Medicine, 2012. **4**(138).
12. Olinger, G.G., et al., *Delayed treatment of Ebola virus infection with plant-derived monoclonal antibodies provides protection in rhesus macaques*. Proceedings of the National Academy of Sciences of the United States of America, 2012. **109**(44): p. 18030-18035.

Chapter IV

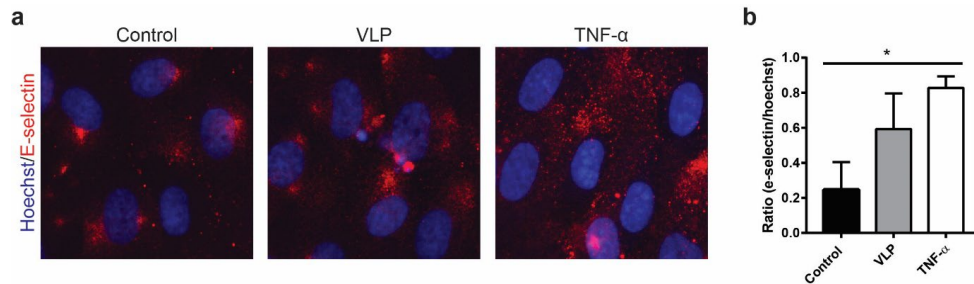
13. Wilson, J.A., et al., *Epitopes involved in antibody-mediated protection from Ebola virus*. Science, 2000. **287**(5458): p. 1664-1666.
14. Thi, E.P., et al., *Lipid nanoparticle siRNA treatment of Ebola-virus-Makona-infected nonhuman primates*. Nature, 2015. **521**(7552): p. 362-+.
15. Munoz, A., et al., *Synthesis of giant globular multivalent glycofullerenes as potent inhibitors in a model of Ebola virus infection*. Nature Chemistry, 2016. **8**(1): p. 50-57.
16. Mestas, J. and C.C.W. Hughes, *Of mice and not men: Differences between mouse and human immunology*. Journal of Immunology, 2004. **172**(5): p. 2731-2738.
17. Reardon, S., *'Organs-on-chips' go mainstream*. Nature, 2015. **523**(7560): p. 266-266.
18. Junaid, A., et al., *An end-user perspective on Organ-on-a-Chip: Assays and usability aspects*. Current Opinion in Biomedical Engineering, 2017. **1**: p. 15-22.
19. Tejavibulya, N. and S.K. Sia, *Personalized Disease Models on a Chip*. Cell Systems, 2016. **3**(5): p. 416-418.
20. Huh, D., et al., *A Human Disease Model of Drug Toxicity-Induced Pulmonary Edema in a Lung-on-a-Chip Microdevice*. Science Translational Medicine, 2012. **4**(159).
21. Park, J., et al., *Three-dimensional brain-on-a-chip with an interstitial level of flow and its application as an in vitro model of Alzheimer's disease*. Lab on a Chip, 2015. **15**(1): p. 141-150.
22. Wang, L., et al., *A disease model of diabetic nephropathy in a glomerulus-on-a-chip microdevice*. Lab on a Chip, 2017. **17**(10): p. 1749-1760.
23. Jeon, J.S., et al., *Generation of 3D functional microvascular networks with human mesenchymal stem cells in microfluidic systems*. Integrative Biology, 2014. **6**(5): p. 555-563.
24. Qiu, Y.Z., et al., *Microvasculature-on-a-chip for the long-term study of endothelial barrier dysfunction and microvascular obstruction in disease*. Nature Biomedical Engineering, 2018. **2**(6): p. 453-463.
25. van Duinen, V., et al., *96 perfusable blood vessels to study vascular permeability in vitro*. Scientific Reports, 2017. **7**.
26. Kim, S., et al., *Engineering of functional, perfusable 3D microvascular networks on a chip*. Lab on a Chip, 2013. **13**(8): p. 1489-1500.
27. Smith, Q. and S. Gerecht, *Going with the flow: microfluidic platforms in vascular tissue engineering*. Current Opinion in Chemical Engineering, 2014. **3**: p. 42-50.
28. Tien, J., *Microfluidic approaches for engineering vasculature*. Current Opinion in Chemical Engineering, 2014. **3**: p. 36-41.

29. Sato, M., et al., *Microcirculation-on-a-Chip: A Microfluidic Platform for Assaying Blood- and Lymphatic-Vessel Permeability*. Plos One, 2015. **10**(9).
30. Bersini, S. and M. Moretti, *3D functional and perfusable microvascular networks for organotypic microfluidic models*. Journal of Materials Science-Materials in Medicine, 2015. **26**(5).
31. Chen, M.B., et al., *On-chip human microvasculature assay for visualization and quantification of tumor cell extravasation dynamics*. Nature Protocols, 2017. **12**(5): p. 865-880.
32. Hovell, C.M., Y.J. Sei, and Y. Kim, *Microengineered Vascular Systems for Drug Development*. Jala, 2015. **20**(3): p. 251-258.
33. Takei, T., S. Sakai, and M. Yoshida, *In vitro formation of vascular-like networks using hydrogels*. Journal of Bioscience and Bioengineering, 2016. **122**(5): p. 519-527.
34. Rayner, S.G. and Y. Zheng, *Engineered Microvessels for the Study of Human Disease*. Journal of Biomechanical Engineering-Transactions of the Asme, 2016. **138**(11).
35. Kim, S., et al., *Vasculature-On-A-Chip for In Vitro Disease Models*. Bioengineering (Basel), 2017. **4**(1).
36. Haase, K. and R.D. Kamm, *Advances in on-chip vascularization*. Regenerative Medicine, 2017. **12**(3): p. 285-302.
37. Akbari, E., G.B. Spychalski, and J.W. Song, *Microfluidic approaches to the study of angiogenesis and the microcirculation*. Microcirculation, 2017. **24**(5).
38. Shin, M., et al., *Endothelialized networks with a vascular geometry in microfabricated poly(dimethyl siloxane)*. Biomedical Microdevices, 2004. **6**(4): p. 269-278.
39. Song, J.W., et al., *Computer-controlled microcirculatory support system for endothelial cell culture and shearing*. Analytical Chemistry, 2005. **77**(13): p. 3993-3999.
40. Wahl-Jensen, V.M., et al., *Effects of Ebola virus glycoproteins on endothelial cell activation and barrier function*. Journal of Virology, 2005. **79**(16): p. 10442-10450.
41. Tasaka, S., et al., *Attenuation of endotoxin-induced acute lung injury by the Rho-associated kinase inhibitor, Y-27632*. American Journal of Respiratory Cell and Molecular Biology, 2005. **32**(6): p. 504-510.
42. Li, Y., et al., *Fasudil attenuates lipopolysaccharide-induced acute lung injury in mice through the Rho/Rho kinase pathway*. Medical Science Monitor, 2010. **16**(4): p. Br112-Br118.
43. Suzuki, K., et al., *Fasudil, a Rho-kinase inhibitor, attenuates lipopolysaccharide-induced vascular hyperpermeability and colonic muscle relaxation in guinea pigs*. Journal of Surgical Research, 2012. **178**(1): p. 352-357.

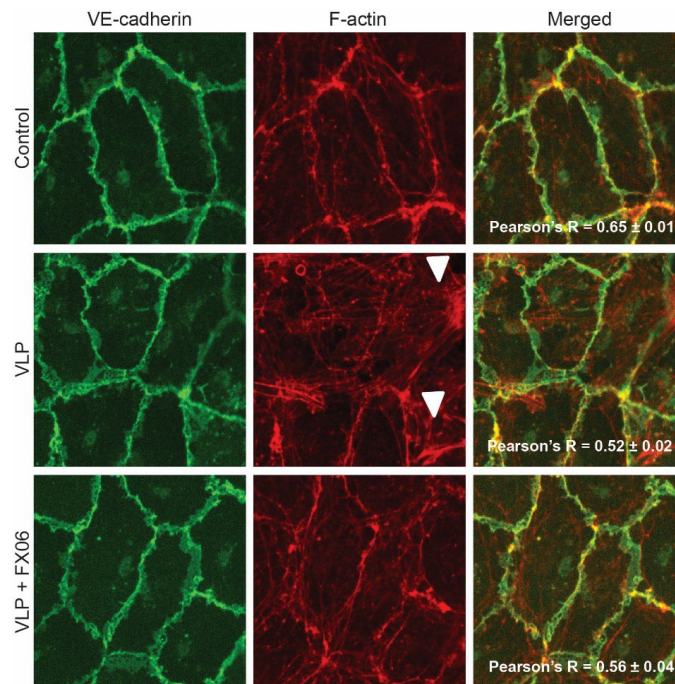
44. Mahanty, S. and M. Bray, *Pathogenesis of filoviral haemorrhagic fevers*. Lancet Infectious Diseases, 2004. **4**(8): p. 487-498.
45. Bray, M. and S. Mahanty, *Ebola hemorrhagic fever and septic shock*. Journal of Infectious Diseases, 2003. **188**(11): p. 1613-1617.
46. Eisa-Beygi, S. and X.Y. Wen, *Could pharmacological curtailment of the RhoA/Rho-kinase pathway reverse the endothelial barrier dysfunction associated with Ebola virus infection?* Antiviral Research, 2015. **114**: p. 53-56.
47. Kobayashi, K., et al., *Thromboxane A(2) exacerbates acute lung injury via promoting edema formation*. Scientific Reports, 2016. **6**.
48. Hansen, M., et al., *Efficient production of erythroid, megakaryocytic and myeloid cells, using single cell-derived iPSC colony differentiation*. Stem Cell Research, 2018. **29**: p. 232-244.
49. Mohan, G.S., et al., *Less Is More: Ebola Virus Surface Glycoprotein Expression Levels Regulate Virus Production and Infectivity*. Journal of Virology, 2015. **89**(2): p. 1205-1217.
50. Bergt, S., et al., *The Fibrin-Derived Peptide B beta(15-42) (FX06) Ameliorates Vascular Leakage and Improves Survival and Neurocognitive Recovery: Implications From Two Animal Models of Cardiopulmonary Resuscitation*. Critical Care Medicine, 2016. **44**(10): p. E988-E995.
51. Uyeki, T.M., et al., *Clinical Management of Ebola Virus Disease in the United States and Europe*. New England Journal of Medicine, 2016. **374**(7): p. 636-646.
52. Petzelbauer, P., et al., *The fibrin-derived peptide Bbeta15-42 protects the myocardium against ischemia-reperfusion injury*. Nat Med, 2005. **11**(3): p. 298-304.
53. Groger, M., et al., *Peptide Bbeta(15-42) preserves endothelial barrier function in shock*. PLoS One, 2009. **4**(4): p. e5391.
54. Roesner, J.P., et al., *Bbeta15-42 (FX06) reduces pulmonary, myocardial, liver, and small intestine damage in a pig model of hemorrhagic shock and reperfusion*. Crit Care Med, 2009. **37**(2): p. 598-605.
55. Wolf, T., et al., *Severe Ebola virus disease with vascular leakage and multiorgan failure: treatment of a patient in intensive care*. Lancet, 2015. **385**(9976): p. 1428-1435.
56. Borin, T.F., et al., *Melatonin decreases breast cancer metastasis by modulating Rho-associated kinase protein-1 expression*. Journal of Pineal Research, 2016. **60**(1): p. 3-15.
57. Tang, S.T., et al., *Melatonin Attenuates Aortic Endothelial Permeability and Arteriosclerosis in Streptozotocin-Induced Diabetic Rats: Possible Role of MLCK- and MLCP-Dependent MLC Phosphorylation*. Journal of Cardiovascular Pharmacology and Therapeutics, 2016. **21**(1): p. 82-92.
58. Tan, D.X., et al., *Ebola virus disease: potential use of melatonin as a treatment*. Journal of Pineal Research, 2014. **57**(4): p. 381-384.

59. Masters, A., et al., *Melatonin, the Hormone of Darkness: From Sleep Promotion to Ebola Treatment*. Brain Disord Ther, 2014. **4**(1).
60. Wiwanitkit, V., *Ebola Virus Infection: What Should Be Known?* North American Journal of Medical Sciences, 2014. **6**(11): p. 549-552.
61. Chahbouni, M., et al., *Melatonin treatment normalizes plasma pro-inflammatory cytokines and nitrosative/oxidative stress in patients suffering from Duchenne muscular dystrophy*. Journal of Pineal Research, 2010. **48**(3): p. 282-289.
62. Escudero-Perez, B., et al., *Shed GP of Ebola Virus Triggers Immune Activation and Increased Vascular Permeability*. Plos Pathogens, 2014. **10**(11).
63. Lyon, G.M., et al., *Clinical Care of Two Patients with Ebola Virus Disease in the United States*. New England Journal of Medicine, 2014. **371**(25): p. 2402-2409.
64. Bah, E.I., et al., *Clinical Presentation of Patients with Ebola Virus Disease in Conakry, Guinea*. New England Journal of Medicine, 2015. **372**(1): p. 40-47.
65. Boral, B.M., D.J. Williams, and L.I. Boral, *Disseminated Intravascular Coagulation*. American Journal of Clinical Pathology, 2016. **146**(6): p. 670-680.
66. Urbchat, A., et al., *The Small Fibrinopeptide B beta(15-42) as Renoprotective Agent Preserving the Endothelial and Vascular Integrity in Early Ischemia Reperfusion Injury in the Mouse Kidney*. Plos One, 2014. **9**(1).
67. Yang, X.P., et al., *Ameliorative effect of melatonin against increased intestinal permeability in diabetic rats: possible involvement of MLCK-dependent MLC phosphorylation*. Molecular and Cellular Biochemistry, 2016. **416**(1-2): p. 23-32.
68. Sanchez-Barcelo, E.J., et al., *Clinical Uses of Melatonin: Evaluation of Human Trials*. Current Medicinal Chemistry, 2010. **17**(19): p. 2070-2095.
69. Kucukakin, B., et al., *Utility of melatonin to treat surgical stress after major vascular surgery - a safety study*. Journal of Pineal Research, 2008. **44**(4): p. 426-431.
70. Gitto, E., et al., *Melatonin reduces oxidative stress in surgical neonates*. Journal of Pediatric Surgery, 2004. **39**(2): p. 184-188.
71. Saphire, E.O., et al., *Antibody-mediated protection against Ebola virus*. Nat Immunol, 2018. **19**(11): p. 1169-1178.
72. Saphire, E.O., et al., *Systematic Analysis of Monoclonal Antibodies against Ebola Virus GP Defines Features that Contribute to Protection*. Cell, 2018. **174**(4): p. 938-952 e13.
73. Dunning, J. and W. Fischer, *Ebola: the battle plan must include specific treatments*. Lancet, 2015. **385**(9976): p. 1373-1375.

Supplementary figures



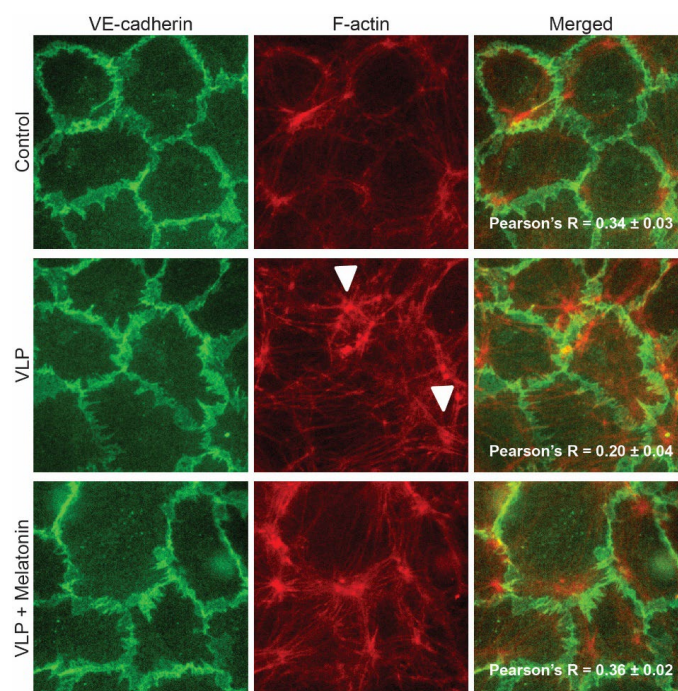
Supplementary figure 1 | Ebola VLPs elevated E-selectin in microvessels. (a) Immunofluorescence for E-selectin expression (red) patterns in an untreated microvessel, 1 $\mu\text{g}/\text{ml}$ Ebola VLP-infected microvessels or 10 ng/ml TNF- α -treated microvessels for 18 h. **(b)** Quantitative determination of E-selectin expression in the absence (control) and presence of 1 $\mu\text{g}/\text{ml}$ Ebola VLPs or 100 ng/ml TNF- α for 2 h. Data are represented as mean \pm SEM. A marginally significant difference ($*P < 0.1$) between the three conditions was found.



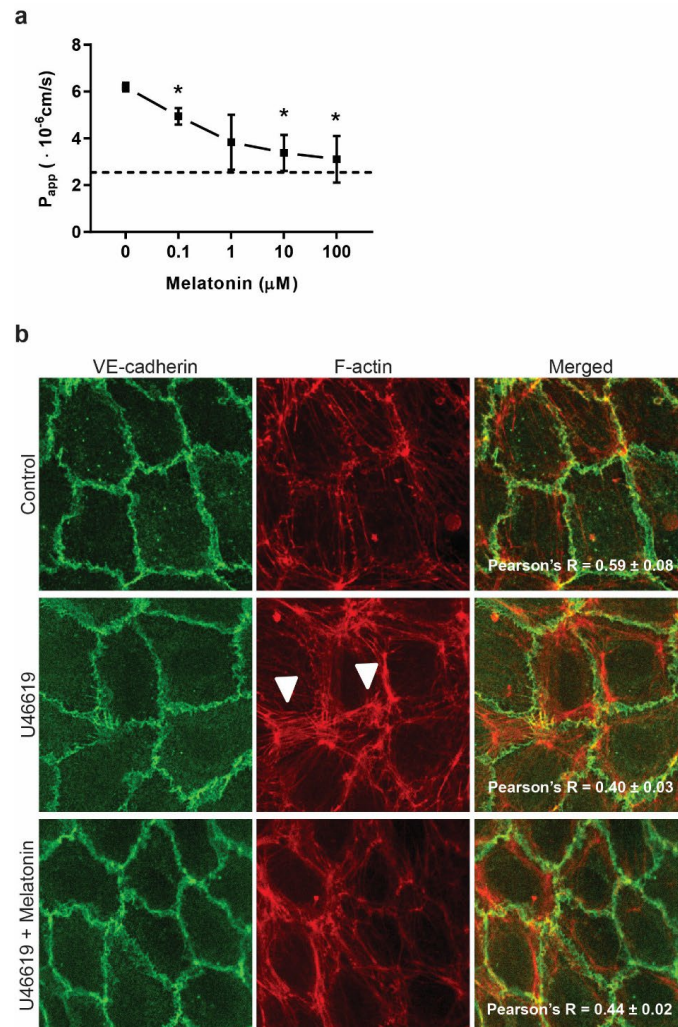
Supplementary figure 2 | Endothelial cells stained for VE-cadherin (green) and F-actin (red) after exposure to 1 $\mu\text{g}/\text{ml}$ VLPs with or without 100 ng/ml FX06 for 2 h. A moderate increase in actin stress fiber formation was observed in microvessels exposed to Ebola VLPs (arrowheads). This increase was abrogated by FX06 treatment.

Chapter IV

Pearson's correlation coefficient was used to quantify the co-localization of VE-cadherin and junction-associated actin filaments. Data are represented as mean \pm SEM.

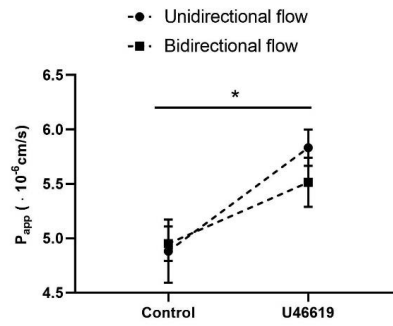


Supplementary figure 3 | Immunostaining of endothelial cells for VE-cadherin (green) and F-actin (red) after exposure to 1 $\mu\text{g}/\text{ml}$ of VLPs with or without 10 μM melatonin for 2 h. A moderate increase in actin stress fiber formation was observed in microvessels incubated with Ebola VLPs (arrowheads). Treatment with melatonin reduced actin stress fiber formation. Pearson's correlation coefficient was used to quantify the co-localization of VE-cadherin and junction-associated actin filaments. Data are represented as mean \pm SEM.



Supplementary figure 4 | Melatonin reduced vascular permeability in U46619-treated microvessels. (a) Microvessels exposed to 10 μM U46619 were treated with the indicated concentrations of melatonin for 1 h. Subsequently, a permeability assay was carried out. **(b)** Endothelial cells stained for VE-cadherin (green) and F-actin (red) after exposure to 10 μM U46619 with or without 10 μM melatonin for 1 h. A moderate increase in actin stress fiber formation was observed in microvessels incubated with U46619 (arrowheads). This increase was abrogated by melatonin treatment. Pearson's correlation coefficient was used to quantify the co-localization of VE-cadherin and junction-associated actin filaments. Data are represented as mean ± SEM.

Chapter IV



Supplementary figure 5 | U46619 induces leakage irrespective of the directionality of the flow within the microvessels. The microvessels were incubated with 10 μ M U46619 and perfused under unidirectional and bidirectional flow for 8 minutes, following a permeability assay. We did not observe a statistically significant difference between the two flow conditions. The data is generated using 42 chips, including 21 control chips and 21 U46619 chips. Data are represented as mean \pm SEM.

IV